MHD ballooning instability in the plasma sheet

C. Z. Cheng
Princeton Plasma Physics Laboratory, Princeton University, Princeton, New Jersey, USA

S. Zaharia
Los Alamos National Laboratory, Los Alamos, New Mexico, USA

Received 11 October 2003; revised 24 November 2003; accepted 16 January 2004; published 23 March 2004.

[1] Based on the ideal MHD model the stability of ballooning modes is investigated by employing realistic 3D magnetospheric equilibria for the substorm growth phase. Our results show that without making compressibility approximations the ballooning modes are unstable for the entire plasma sheet where the equatorial $\beta_{eq} \geq 1$, and the most unstable modes are located in the strong cross-tail current sheet region in the near-Earth plasma sheet, which maps to the initial brightening location of the breakup arc in the ionosphere. However, the MHD β_{eq} threshold is too low in comparison with observations by AMPTE/CCE, which show that prior to substorm onset a low frequency instability is excited only when $\beta_{eq} > 50$. The difficulty can be mitigated by including kinetic effects, which greatly increase the stabilizing effects of field line tension and can enhance the β_{eq} threshold to limit the unstable region to the cross-tail current sheet region. *INDEX TERMS:* 2740 Magnetospheric Physics: Magnetospheric configuration and dynamics; 2752 Magnetospheric Physics: MHD waves and instabilities; 2753 Magnetospheric Physics: Numerical modeling; 2764 Magnetospheric Physics: Plasma sheet; 2788 Magnetospheric Physics: Storms and substorms. **Citation:** Cheng, C. Z., and S. Zaharia (2004), MHD ballooning instability in the plasma sheet, *Geophys. Res. Lett.*, *31*, L06809, doi:10.1029/2003GL018823.

1. Introduction

[2] Observations by AMPTE/CCE satellite have demonstrated that toward the end of late growth phase the plasma pressure in the near-Earth plasma sheet region becomes isotropic and the equatorial $\beta_{eq} = 2P/B_{eq}^2$ increases to $\geq$50 and a low frequency instability with a wave period of $\sim$50–75 seconds (in the Pi 2 frequency range) is excited and grows exponentially to a large amplitude and causes the onset of current disruption [*Cheng and Lui*, 1998]. It is emphasized that the initial excitation of the low frequency instability occurs in a localized equatorial area of less than 1 R_E in width in the near-Earth plasma sheet region. The low frequency modes have also been observed by satellites near the initiation region during the substorm expansion phase [e.g., *Roux et al.*, 1991; *Erickson et al.*, 2000].

[3] To explain the observed low frequency instability, theoretical investigations of the ballooning instability based on the ideal MHD model have been made [e.g., *Lee and Wolf*, 1992; *Hurricane*, 1997; *Bhattacharjee et al.*, 1998; *Lee*, 1998; *Horton et al.*, 1999; *Lee*, 1999]. All these previous MHD calculations employed simplified equilibria in 2D geometries and made simplified assumptions on the plasma compressibility. Numerical calculations to examine the compressibility effect with different simplifying assumptions of the plasma compressibility have been performed [*Lee*, 1999] for a 2D equilibrium developed by *Voigt* [1986]. By assuming the parallel plasma displacement to be a constant along the field line [*Lee and Wolf*, 1992], the stability calculations predicted a low β ($\pm$ 1) threshold for instability. *Horton et al.* [1999] considered a different approximation for the plasma compressibility with the fast-MHD model which assumes that the wave propagates very fast along the ambient magnetic field such that there is not sufficient time for parallel plasma motion and the plasma displacement along **B** vanishes, and they concluded that the ballooning instability occurs for $\beta < 1$. However, the numerical stability calculations of the fast-MHD model performed by *Lee* [1999] show that the ballooning mode is stable in the Voigt's equilibrium, which is in contradiction to the analytical conclusion of *Horton et al.* [1999]. Calculations with these simplifying compressibility models, but with a more stretched 2D equilibrium field model by *Kan* [1973] gave totally different results from the Voigt's equilibrium. These results clearly illustrate that to obtain the correct stability result even within the ideal MHD model it is essential to model the plasma compressibility correctly as well as the equilibrium fields realistically. Another drawback of these previous ballooning stability calculations is that there is no information on where in the equatorial plane the ballooning instability would be unstable because of the use of 2D equilibria.

[4] In this paper we will investigate the ballooning instability based on the ideal MHD model without making assumptions on plasma compressibility. Moreover, we will employ realistic 3D growth phase magnetospheric equilibria that satisfy the force balance, which should provide the valuable information of where in the plasma sheet the free energy and the most unstable ballooning instability are located. Our results show that the ballooning stability calculations making use of approximations on the plasma compressibility can give rise to erroneous conclusions. Moreover, our results show that the ballooning instability is most unstable in the strong cross-tail current sheet region in the near-Earth plasma sheet, which maps to the initial brightening location of the breakup arc in the ionosphere.

2. MHD Ballooning Mode Theory

[5] We first derive the ideal MHD eigenmode equations (in rationalized EMU system of units) without making

Copyright 2004 by the American Geophysical Union.
0094-8276/04/2003GL018823$05.00

assumption on the plasma compressibility. We consider quasi-static isotropic pressure equilibria with the equilibrium relation $\mathbf{j} \times \mathbf{B} = \nabla P$, where $\mathbf{j}$, $\mathbf{B}$, P are the equilibrium current density, magnetic field, and plasma pressure, respectively. With the time dependence of perturbed quantities as $e^{-i\omega t}$, we obtain simplified eigenmode equations for perturbations with $k_\perp \gg k_\parallel$ where $k_\perp$ and $k_\parallel$ are the wave numbers perpendicular and parallel to $\mathbf{B}$, respectively. We introduce the electrostatic potential ϕ and the vector potential $\mathbf{A}$ such that the perturbed electric field is expressed as $\delta\mathbf{E} = -\nabla\phi + i\omega\mathbf{A}$, and the perturbed magnetic field as $\delta\mathbf{B} = \nabla \times \mathbf{A}$. Because $\delta\mathbf{E} \cdot \mathbf{B} = 0$ in the ideal MHD model, $A_\parallel = \mathrm{A} \cdot \mathbf{B}/B = -\mathbf{B} \cdot \nabla\Phi/B$, where $\Phi = i\phi/\omega$. By assuming that $A_\parallel$ and $\mathbf{A}_\perp$ are of the same order, $\delta\mathbf{E}_\perp \simeq -\nabla_\perp\phi$, where the $\mathbf{A}_\perp$ term is ignored because it is smaller by $k_\parallel/k_\perp$. Then, $\boldsymbol{\xi} \times \mathbf{B} \simeq \nabla_\perp \Phi$, where $\boldsymbol{\xi}$ is the plasma fluid displacement vector. Following the procedures described in the papers by *Cheng* [1991] and *Cheng and Johnson* [1999] and considering the wave frequency to be much smaller than the compressional wave frequency, we obtain two coupled equations that describe the coupling between the shear Alfvén type modes and the slow magnetosonic type modes: the vorticity equation for the shear Alfvén wave branch:

$$\mathbf{B} \cdot \nabla\left(\frac{\nabla_\perp^2(\mathbf{B} \cdot \nabla\Phi)}{B^2}\right) + \frac{\rho\omega^2}{B^2}\nabla_\perp^2\Phi - \frac{2\boldsymbol{\kappa} \times \mathbf{B}}{B^2} \cdot \nabla\left(\frac{\mathbf{B} \times \nabla P \cdot \nabla\Phi}{B^2}\right) = \frac{2\boldsymbol{\kappa} \times \mathbf{B}}{B^2}\nabla \cdot (\Gamma_s P \nabla\boldsymbol{\xi}), \quad (1)$$

and the compressibility equation for the slow magnetosonic mode branch:

$$\mathbf{B} \cdot \nabla\left[\frac{\Gamma_s P}{\rho\omega^2 B^2}\mathbf{B} \cdot \nabla(\nabla \cdot \boldsymbol{\xi})\right] + \frac{\Gamma_s P + B^2}{B^2}\nabla \cdot \boldsymbol{\xi} = \frac{2\boldsymbol{\kappa} \times \mathbf{B}}{B^2}\nabla\Phi. \quad (2)$$

where ρ is the mass density, and the coupling is mainly via the magnetic field curvature $\boldsymbol{\kappa} = (\mathbf{B}/B) \cdot \nabla(\mathbf{B}/B)$ and the plasma pressure.

2.1. MHD Ballooning Mode Equations

[6] Equations (1) and (2) describe low frequency modes in the three-dimensional space and are usually difficult to solve if not impossible. Thus, further approximations must be made to simplify these two equations. Fortunately a WKB-ballooning formalism has been developed to simplify these equations by taking advantage of the nature of solutions that $k_\perp \gg k_\parallel$ [*Dewar and Glasser*, 1983; *Nevins and Pearlstein*, 1988]. Adopting the WKB-ballooning formalism, we consider the eikonal representation of the perturbed quantities, $\Phi = i\, e^{iS}\hat{\Phi}$, where $S \gg 1$ is the WKB eikonal and $\mathbf{B} \cdot \nabla S = 0$. Note that ∇S is essentially the wave vector perpendicular to $\mathbf{B}$. Thus, the fast variation of Φ in the direction perpendicular to $\mathbf{B}$ is contained in e^{iS} and $\hat{\Phi}$ describes the slow variation along as well as perpendicular to $\mathbf{B}$. Then, to the lowest order in $1/S \ll 1$, the MHD vorticity equation, Equation (1), reduces to

$$\mathbf{B} \cdot \nabla\left(\frac{|\nabla S|^2\mathbf{B} \cdot \nabla\hat{\Phi}}{B^2}\right) + \frac{\rho\omega^2}{B^2}|\nabla S|^2\hat{\Phi} + \kappa_c P_s\hat{\Phi} + \kappa_c(\Gamma_s P\Delta) = 0, \quad (3)$$

where $\kappa_c = 2\boldsymbol{\kappa} \times \mathbf{B} \cdot \nabla S/B^2$, $P_s = \nabla P \times \mathbf{B} \cdot \nabla S/B^2$, and $\nabla \cdot \boldsymbol{\xi} = e^{iS}\Delta$. Similarly, Equation (2) reduces to

$$\mathbf{B} \cdot \nabla\left[\frac{\Gamma_s P}{\rho\omega^2 B^2}\mathbf{B} \cdot \nabla\Delta\right] + \frac{\Gamma_s P + B^2}{B^2}\Delta + \kappa_c\hat{\Phi} = 0. \quad (4)$$

equations (3) and (4) are 1D equations along $\mathbf{B}$, and the eigenvalues depend on the angle between ∇S and ∇P. With the Euler potential representation of the ambient magnetic field $\mathbf{B} = \nabla\psi \times \nabla\alpha$, ∇S can be expressed as $\nabla S = S_\psi\nabla\psi + S_\alpha\nabla\alpha$, where $S_\psi = \partial S/\partial\psi$, and $S_\alpha = \partial S/\partial\alpha$. Then, $\kappa_c = 2S_\alpha[\kappa_s(\nabla\psi \cdot \nabla\alpha/|\nabla\psi|^2 + \Upsilon/\psi) - \kappa_\psi]$, and $P_s = S_\alpha[(\Upsilon/\psi)\partial P/\partial\alpha - \partial P/\partial\psi]$, where $\kappa_\psi = \boldsymbol{\kappa} \cdot \nabla\psi/|\nabla\psi|^2$, $\kappa_s = \boldsymbol{\kappa} \cdot \mathbf{B} \times \nabla\psi/\mathrm{B}^2$, and $\Upsilon = \psi\, S_\psi/S_\alpha$ is a dimensionless free parameter. Note that S_α can be combined with $\hat{\Phi}$, and equations (3) and (4) depend on Υ. Thus, the eigenvalue, ω^2, is a function of Υ for each field line labeled by ψ and α. In the following we present numerical solutions of equations (3) and (4) by choosing $\Upsilon = 0$, which corresponds to the most unstable solutions.

[7] To solve equations (3) and (4), we construct a variational principle, and the Lagrangian functional δL is given by

$$\delta L = \int_{s_1}^{s_2}\frac{ds}{B}\left\{\rho\omega^2\left(\frac{|\nabla S|^2}{B^2}|\hat{\Phi}|^2 + B^2|Z|^2\right) + \kappa_c P_s|\hat{\Phi}|^2 - \left[\frac{|\nabla S|^2}{B^2}|\mathbf{B} \cdot \nabla\hat{\Phi}|^2 + \frac{\Gamma_s P B^2}{\Gamma_s P + B^2}|\kappa_c\hat{\Phi} + \mathbf{B} \cdot \nabla Z|^2\right]\right\} = 0 \quad (5)$$

where s denotes the distance along the field line, s_1 and s_2 are the two end points of the field line anchored in the ionosphere, $Z = \Gamma_s P\,(\mathbf{B} \cdot \nabla\Delta)/\rho\omega^2 B^2$. The boundary conditions at the field line end points are assumed to be $\hat{\Phi}^*\mathbf{B} \cdot \nabla\hat{\Phi} = 0$ and $\Delta Z^* = 0$. It is noted from Equation (5) that there is a possibility of $\omega^2 < 0$ if $\kappa_c P_s > 0$, and if $\omega^2 < 0$ the plasma is unstable at these field lines. From the definition of κ_c and P_s (given after Equation (3)) we see that if the pressure gradient is in the same direction as the magnetic field curvature, then $\kappa_c P_s > 0$ and the ballooning mode is possible to be unstable.

2.2. Numerical Solutions

[8] To obtain the mode frequency or growth rate in physical unit we need to specify the mass density distribution. For simplicity the plasma density is chosen to be constant along the field line, but is a function of radius in the equatorial plane: $\rho(R) = 10\,(R_{geos}/R)^3 m_p/cm^3$, where $R_{geos} = 6.6\,R_E$ and m_p is the proton mass. When the actual mass density distribution is known, the frequency or growth rate can be recalculated from the results given in this paper.

[9] Employing the growth phase magnetospheric equilibrium published previously [*Zaharia and Cheng*, 2003] and choosing $\Upsilon = 0$, we compute numerically the eigenvalues ω^2 and the eigenfunctions by solving the Lagrangian equation, Equation (5), for each field line with the boundary conditions that both $\hat{\Phi}$ and Δ vanish at the end points of the field line in the ionosphere. Figures 1 and 2 show the color plots in the equatorial plane and the contours in the northern polar ionosphere of the eigenvalue f^2 (in $(\mathrm{mHz})^2$) for the fundamental harmonic ballooning modes, respectively. Also shown in Figure 1 are the contours of the azimuthal current

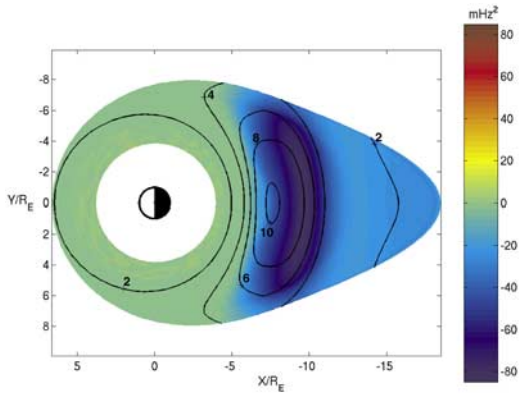

Figure 1. The square of ballooning mode frequency (in $(\mathrm{mHz})^2$) is shown in the equatorial plane with the full MHD model. The azimuthal current density (in $\mathrm{nA/m^2}$) contours are also plotted to show the location of the most unstable region relative to the strong cross-tail current region.

density (in $\mathrm{nA/m^2}$) and in Figure 2 is the color plot of the field-aligned current density. Note that all field lines beyond $x \simeq -6\ \mathrm{R_E}$ down the tail in the night side are unstable. The region of the most unstable modes tracks well with the strong cross-tail current sheet region, consistent with the expectation from substorm onset observations. The peak growth rate region is located in the tailward side of the strong cross-tail current region. In the polar ionosphere the field lines in the peak ballooning instability growth rate region map to the transition region between the region-1 and region-2 currents. Although the ideal MHD model over estimates the instability growth rate due to the lack of particle kinetic effects [*Cheng and Lui*, 1998], the results show the field lines where the ballooning free energy is largest and the most unstable ballooning mode is located. Moreover, we expect that the global structure of the MHD ballooning instability is localized around the maximum growth rate location in the equatorial plane with an half-width extending to the location with growth rate equal to about one half of the maximum growth rate.

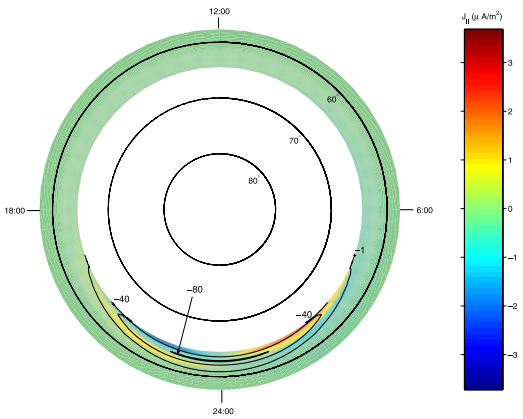

Figure 2. The contours of the square of ballooning mode frequency (in $(\mathrm{mHz})^2$) are plotted over the northern polar ionosphere for the full MHD model. The field-aligned current density is plotted to show that the most unstable ballooning instability region is located at the transition region between the region-1 and region-2 currents.

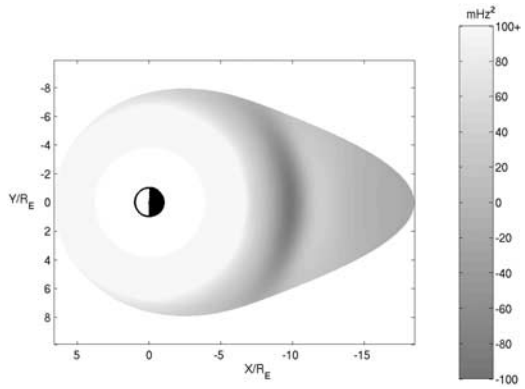

Figure 3. The square of ballooning mode frequency (in $(\mathrm{mHz})^2$) is plotted in the equatorial plane for the Lee-Wolf model.

[10] Next, we compute the stability of the ballooning modes for the same growth phase magnetospheric equilibrium with the Lee-Wolf model [*Lee and Wolf*, 1992] and the fast-MHD model [*Horton et al.*, 1999], which made approximations on the plasma compressibility, and compare these solutions with the solutions of the full MHD model. This will resolve the controversy arising from these approximations [*Lee*, 1999]. In the Lee-Wolf model, the plasma compressibility is assumed to be a non-vanishing constant along the field line. With $\mathbf{B} \cdot \nabla\Delta = 0$, Δ can be obtained from Equation (4) and is given by $<(\Gamma_s P + B^2)/B^2> \Delta + <\kappa_c \hat{\Phi}> = 0$, where $< X > = \int_{s_1}^{s_2} ds X/B$. Then, from Equation (3) we obtain the Lee-Wolf equation as shown in equation (3) of [*Lee*, 1999]. The solution of the Lee-Wolf model, shown in Figure 3, shows that ballooning modes are unstable near the current sheet region between $X = -8$ and $-10\ \mathrm{R_E}$ and weakly unstable farthest near the tail boundary, but are stable in other regions. This result is different from the full MHD solution shown in Figure 1. Thus, the Lee-Wolf model produces too much stabilization due to the approximation of constant plasma compressibility.

[11] In the fast-MHD model [*Horton et al.*, 1999], the parallel displacement is assumed to vanish, $\boldsymbol{\xi} \cdot \mathbf{B} = 0$. From the adiabatic pressure law and the parallel component of the momentum equation, we obtain $\Delta + [\kappa_c B^2/(\Gamma_s P + B^2)]\hat{\Phi} = 0$. Then, from Equation (3) we obtain the fast-MHD equation shown in equation (8) of [*Lee*, 1999]. The solution of the fast-MHD model, shown in Figure 4, clearly shows that for most field lines (except farthest in the tail of the equilibrium) the ballooning modes are stable. This result is completely different from the results of the full MHD model shown in Figures 1 and those of the Lee-Wolf model shown in Figure 3. Thus, the fast-MHD model gives a much worse approximation of the plasma compressibility.

3. Summary and Discussion

[12] In summary, based on the ideal MHD model the ballooning modes are expected to be unstable for the growth phase magnetospheric equilibrium in a large region of the plasma sheet where $\beta_{eq} \geq 1$. The most unstable region is located in the strong cross-tail current sheet

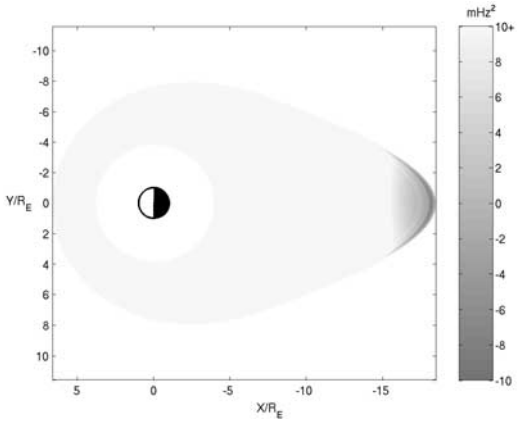

Figure 4. The square of ballooning mode frequency (in $(\mathrm{mHz})^2$) is plotted in the equatorial plane for the fast-MHD model.

region, which maps into the ionosphere in the transition area between the region-1 and region-2 currents. The numerical results clearly illustrate that to obtain the correct stability result even within the ideal MHD model it is essential to model the plasma compressibility correctly as well as the equilibrium fields realistically.

[13] The results of the ideal MHD ballooning mode stability calculations are not consistent with the AMPTE/CCE observations that during most of the growth phase $\beta_{eq} < 50$ and the magnetic fields are quiet without noticeable fluctuations [*Lui et al.*, 1992], and the low frequency instability was observed in the enhanced cross-tail current sheet region only toward the end of the growth phase when $\beta_{eq} > 50$ [*Cheng and Lui*, 1998]. Moreover, the ideal MHD model would predict purely growing ballooning instabilities, and thus cannot explain the observed frequency of the instability. Another fundamental difficulty of the ideal MHD model is that there is no parallel electric field, and thus the unstable MHD ballooning mode does not accelerate particles to produce the substorm onset auroral brightening as observed in the ionosphere. However, even with these inconsistencies with observations, the ideal MHD model provides the valuable information that the most unstable ballooning instability is located in the strong cross-tail current sheet region.

[14] To mitigate these difficulties arising from the ideal MHD model, we need to consider the particle kinetic effects. As was shown previously [*Cheng and Lui*, 1998], the kinetic effects of ion gyroradii and trapped electron dynamics can greatly increase the stabilizing effects of field line tension and thus enhance the critical β to excite the ballooning instability. The consequence is to reduce the equatorial region of the unstable ballooning modes to the strong cross-tail current sheet region. Full kinetic calculations need to be carried out to provide a quantitative conclusion.

[15] **Acknowledgments.** This work is supported by the NASA grant No. W-10062 and the DoE Contract No. DE-AC02-76-CHO3073.

References

Bhattacharjee, A., Z. W. Ma, and X. Wang (1998), Ballooning instability of a thin current sheet in the high Lundquist-number magnetotail, *Geophys. Res. Lett.*, *25*(6), 861–864.

Cheng, C. Z. (1991), A kinetic-magnetohydrodynamic model for low-frequency phenomena, *J. Geophys. Res.*, *96*(A12), 21,159–21,171.

Cheng, C. Z., and J. R. Johnson (1999), A kinetic-fluid model, *J. Geophys. Res.*, *104*(A1), 413–428.

Cheng, C. Z., and A. T. Y. Lui (1998), Kinetic ballooning instability for substorm onset and current disruption observed by AMPTE/CCE, *Geophys. Res. Lett.*, *25*(21), 4091–4094.

Dewar, R. L., and A. H. Glasser (1983), Ballooning mode spectrum in general toroidal systems, *Phys. Fluids*, *26*, 3038.

Erickson, G. M., N. C. Maynard, W. J. Burke, G. R. Wilson, and M. A. Heinemann (2000), Electromagnetics of substorm onsets in the near-geosynchronous plasma sheet, *J. Geophys. Res.*, *105*(A11), 25,265–25,290.

Horton, W., H. V. Wong, and J. V. Van Dam (1999), Substorm trigger conditions, *J. Geophys. Res.*, *104*(A10), 22,745–22,758.

Hurricane, O. A. (1997), MHD ballooning stability of a sheared plasma sheet, *J. Geophys. Res.*, *102*(A9), 19,903–19,912.

Kan, J. (1973), On the structure of the magnetotail current sheet, *J. Geophys. Res.*, *78*, 3773.

Lee, D. Y. (1998), Ballooning instability in the tail plasma sheet, *Geophys. Res. Lett.*, *25*(21), 4095–4098.

Lee, D. Y. (1999), Effect of plasma compression on plasma sheet stability, *Geophys. Res. Lett.*, *26*(17), 2705–2708.

Lee, D. Y., and R. A. Wolf (1992), Is the Earth's magnetotail balloon unstable?, *J. Geophys. Res.*, *97*(A12), 19,251–19,257.

Lui, A. T. Y., et al. (1992), Current disruptions in the near-Earth neutral sheet region, *J. Geophys. Res.*, *97*(A2), 1461–1480.

Nevins, W. M., and L. D. Pearlstein (1988), Moderate-m ballooning modes in quadrapole stabilized tandem mirrors, *Phys. Fluids*, *31*, 1988.

Roux, A., S. Perraut, A. Morane, P. Robert, A. Korth, G. Kremser, A. Pederson, R. Pellinen, and Z. Y. Pu (1991), Plasma sheet instability related to the westward traveling surge, *J. Geophys. Res.*, *96*(A10), 17,697–17,714.

Voigt, G.-H. (1986), Field line twist and field-aligned currents in an axisymmetric equilibrium magnetosphere, *J. Geophys. Res.*, *91*(A10), 10,995–11,002.

Zaharia, S., and C. Z. Cheng (2003), Near-Earth thin current sheets and Birkeland currents during substorm growth phase, *Geophys. Res. Lett.*, *30*(17), 1883, doi:10.1029/2003GL017456.

C. Z. Cheng, Princeton Plasma Physics Laboratory, Princeton University, Princeton, NJ 08543, USA. (fcheng@pppl.gov)

S. Zaharia, Los Alamos National Laboratory, Los Alamos, NM 87545, USA. (szaharia@lanl.gov)